Author/s:
Cameron, JM;Mito, R;Berkovic, SF;Jackson, GD

Title:
Progressive Myoclonus Epilepsy: Distinctive MRI Changes in Cerebellar and Motor Networks

Date:
2025-06-01

Citation:
Cameron, J. M., Mito, R., Berkovic, S. F. & Jackson, G. D. (2025). Progressive Myoclonus Epilepsy: Distinctive MRI Changes in Cerebellar and Motor Networks. Annals of Clinical and Translational Neurology, 12 (6), pp.1135-1143. https://doi.org/10.1002/acn3.70010.

Persistent Link:
https://hdl.handle.net/11343/362646

Annals of Clinical and Translational Neurology

RESEARCH ARTICLE OPEN ACCESS

Progressive Myoclonus Epilepsy: Distinctive MRI Changes in Cerebellar and Motor Networks

Jillian M. Cameron[1] | Remika Mito[2] | Samuel F. Berkovic[1] | Graeme D. Jackson[2]

[1]Epilepsy Research Centre, Department of Medicine, University of Melbourne, Austin Health, Melbourne, Victoria, Australia | [2]Florey Institute of Neuroscience and Mental Health, Heidelberg, Victoria, Australia

Correspondence: Jillian M. Cameron (jillian.cameron@austin.org.au)

Received: 16 February 2024 | **Revised:** 31 December 2024 | **Accepted:** 28 January 2025

Funding: This work was supported by the National Health and Medical Research Council (1091593 and 1196637) and the Department of Health, State Government of Victoria.

Keywords: motor networks | MRI | progressive myoclonus epilepsy

ABSTRACT

Objective: Progressive myoclonus epilepsy (PME) is a rare generalized epilepsy syndrome with a well-characterized genetic basis. The brain networks that are affected to give rise to the distinctive symptoms of PME are less well understood.

Methods: Eleven individuals with PME with a confirmed genetic diagnosis and 22 controls were studied. MRI included diffusion acquisition using 64 directions, $b = 3000\,s/mm^2$. Fixel-based analysis was used to identify white matter pathways with significant abnormality in structural connectivity, with subsequent tract segmentation and analysis. Region-of-interest and whole-brain volumetric analysis of T1-weighted images was performed. The relationship between structural connectivity measures and disease duration, and Unified Myoclonus Rating Scale was assessed.

Results: Analysis of structural connectivity revealed significantly reduced fiber density and fiber bundle cross-section in white matter tracts in individuals with PME, with the most severe involvement of tracts within the cerebello-thalamo-cortical network, particularly the cerebello-thalamic, thalamo-cortical, cortico-thalamic, and corticospinal tracts, as well as the splenium of the corpus callosum. By comparison with these abnormalities, cortico-cortical association pathways were relatively preserved. There was reduced volume in the cerebellum, thalamus, brainstem, and mid-anterior corpus callosum.

Interpretation: Individuals with PME have atrophy and changes in fiber tracts that predominantly affect the cerebello-thalamic and motor systems, likely reflecting neuronal and axonal loss as part of a degenerative process. This imaging pattern is distinctive and accords well with the characteristic clinical, neuropathological, and neurophysiological features of the PMEs. The mechanism by which the PME genes affect these tracts is not yet known.

1 | Introduction

Progressive myoclonus epilepsy (PME) is a rare generalized epilepsy syndrome, clinically characterized by progressively worsening myoclonus, tonic–clonic seizures, and ataxia [1]. Although a spectrum of severity exists across the various types of PME, overall this syndrome represents one of the most devastating forms of epilepsy. Progressive neurological deterioration is seen, often associated with cognitive decline and neuropsychiatric disturbance. Onset is typically in later childhood or adolescence, and the clinical phenotype can cause significant functional impairment. For most types of PME, there are currently no disease-modifying therapies, and the prognosis is generally poor, with significantly reduced life expectancy.

Recent advances in molecular genetics have improved understanding of the genetic etiology of PME, with a molecular diagnosis reached in approximately 80% of cases [2, 3]. However,

the brain networks that are affected to give rise to the distinctive clinical phenotype of PME are not well understood. Human histopathological data are limited [4, 5]. In the archetypical and most common form of PME, Unverricht Lundborg disease (ULD), there is loss of Purkinje cells in predominantly the posterior lobe of the cerebellum [6]. Animal models show severe loss of cerebellar granule cells due to apoptosis, and gliosis within the hippocampus, entorhinal cortex, neocortex, and striatum [7, 8]. Voxel-based morphometry studies in individuals with ULD have shown volume loss in bilateral cortical motor areas and thalamus [9]. Proton magnetic resonance spectroscopy studies revealed significant brain metabolite abnormalities involving brainstem and cerebellum, basal ganglia, thalamus, insula, and the occipital lobe [10, 11]. Cortical hyperexcitability, demonstrated by increased cortical somatosensory-evoked potentials (giant-evoked potentials) and transcranial magnetic stimulation (TMS) markers of motor excitability (increased intracortical motor excitability), is well established in individuals with PME [12, 13]. However, exact mechanisms or networks generating the characteristic PME phenotype are yet to be elucidated.

To the best of our knowledge, there has been only one study investigating white matter tract abnormalities in humans with PME, limited to participants with ULD [14]. This study, which used diffusion tensor imaging (DTI)-based metrics, reported widespread abnormality throughout white matter tracts. DTI-based metrics (such as fractional anisotropy, mean, and radial diffusivity) are inherently voxel-averaged and cannot provide accurate measures of structural connectivity in voxels containing crossing fiber populations, a situation encountered in most white matter voxels [15]. This may impact the interpretation of results [16]. More advanced diffusion-weighted imaging (DWI) models address this issue by resolving multiple fiber populations within a single voxel. Fixel-based analysis (FBA, where fixel refers to a specific *fi*ber population within a vo*xel*) is an advanced DWI analysis technique, which not only resolves multiple fiber populations within voxels but also ensures that quantitative metrics to be derived for each specific fiber population, thus enabling identification of the specific fiber structures affected, even in crossing fiber regions. No studies to date have investigated white matter pathway abnormalities in PME using advanced DWI analysis models such as FBA.

In this study, we aimed to identify which brain regions and networks are most affected in PME using both FBA and volumetric analysis, hypothesizing that in PME, the most severely affected tracts and brain regions are in the motor system and cerebellum, consistent with the characteristic progressive ataxia and stimulus-sensitive myoclonus.

2 | Methods

2.1 | Participants

Participants with a confirmed diagnosis of PME were recruited through the Austin Hospital (Melbourne, Australia) and from nationwide centers on the basis of previous clinical referrals and review at our center. Inclusion criteria were a clinical diagnosis of PME with a confirmed genetic etiology and no contraindication to having an MRI scan. Twelve subjects were recruited for the study; one subject was not able to tolerate the scan due to the severity of myoclonus, and thus 11 individuals with PME were included in the study. MRI scans were reviewed through visual inspection for all participants to assess data quality.

Healthy control participants were selected from previously acquired DWI control data obtained at our facility. For each case, two healthy controls were selected and matched for sex, age (±7 years), and the MRI scanner on which imaging was obtained. Twenty-two healthy controls were selected.

The Austin Health Human Research Ethics Committee at the Austin Hospital, Melbourne, Australia approved this study (Project No. H2012/04475). Written informed consent was obtained from all participants.

2.2 | Clinical Assessment

Participants with PME were clinically assessed by an epilepsy neurologist (J.C.) immediately prior to MRI scan acquisition. The severity of myoclonus was assessed using the Unified Myoclonus Rating Scale (UMRS), a validated myoclonus assessment scale [17]. To minimize the impact of movement artifact due to myoclonus at the time of MRI acquisition, scans were conducted in a low-stimulus environment, with extra time allowed to facilitate participant acclimatization. A trial run in a mock-scanner environment was offered to all participants. All participants were on their regular antiepileptic medications at the time of imaging.

2.3 | MRI Data Acquisition

MRI data were acquired at 3 T on a Siemens Skyra with a 32-channel head coil receiver (Erlangen, Germany). High angular resolution diffusion imaging (HARDI) data were acquired on the Skyra with the following parameter set (64 diffusion-weighted images at $b = 3000\,s/mm^2$ and 8 $b = 0\,s/mm^2$ images, voxel size = 2.5 mm^3, TR/TE = 8800/110 ms, length of DWI acquisition = 9 min). Isotropic T1-weighted magnetization-prepared rapid acquisition gradient echo (MPRAGE) images (voxel size = 0.9 mm^3, TR/TE = 1900/2.5 ms, inversion time = 900 ms, flip angle = 9°, acquisition matrix = 256 × 256 × 192) were also acquired from all participants for volumetric analysis.

2.4 | DWI Processing

All DWI data were preprocessed and analyzed using MRtrix3 [18]. Preprocessing of diffusion-weighted images included the following steps: denoising [19], Gibbs ringing removal [20], eddy current correction, motion correction, bias field correction [21], and upsampling. Eddy current and motion correction were performed using FSL's "eddy" tool [22].

The potential for motion artifact due to the stimulus-sensitive myoclonus and impaired motoric control associated with PME was recognized and addressed in the analysis. Estimates of single-subject average absolute motion were obtained using

eddy QC tools [23] and included in statistical analysis as a nuisance regressor.

Fiber orientation distribution (FOD) functions were calculated using single-shell 3-tissue constrained spherical deconvolution (SS3T-CSD) using MRtrix3Tissue (https://3Tissue.github.io), a fork of MRtrix3 [18], with group-averaged response functions for white matter, gray matter, and CSF [24]. Joint bias field and intensity normalization were then performed. A study-specific FOD template was created using a randomly selected subset of participants (10 cases, 10 controls). FOD images from all participants were then registered to this unbiased template using FOD-guided, nonlinear registration [25].

The FBA framework was applied, with measures of apparent fiber density (FD), fiber bundle cross-section (FC), and the combined metric of fiber density and cross-section (FDC) obtained for each subject at each white matter fixel.

2.5 | Tract Segmentation

White matter bundle segmentation was performed on the study-specific FOD template using TractSeg [26], with 72 white matter tracts extracted for tract-based post hoc analysis.

2.6 | T1 Imaging Processing

Volumetric analysis was performed using the FreeSurfer v6 image analysis suite (http://surfer.nmr.mgh.harvard.edu) [27]. Volumetric T1-weighted images were automatically processed with the longitudinal stream in FreeSurfer [28]. Subcortical and cerebellar brain structures were segmented automatically from the T1-weighted images. Absolute volumetric data for 16 identified brain regions of interest (ROI), as well as total brain volume and intracranial volume, were calculated using automated methods.

2.7 | Statistical Analysis

2.7.1 | Whole-Brain FBA

Whole-brain fixel-based analyses of fixel-based metrics (FD, FC, and FDC) were performed using a general linear model, comparing individuals with PME to controls. Age, intracranial volume, and estimated participant motion were included as covariates. Family-wise error (FWE)-corrected p values were then assigned to each fixel using nonparametric permutation testing over 5000 permutations. A subgroup whole-brain FBA of the most common type of PME in our cohort (ULD) was also conducted, comparing individuals with ULD to controls.

2.7.2 | White Matter Tract Analysis

To determine the white matter tracts most affected in PME, tract segmentations for each white matter bundle were converted to fixels, and the percentage of significantly affected fixels was calculated (significantly affected fixels/total fixels in a given white matter bundle × 100). We defined severely affected tracts as those tracts with greater than 40% of fixels affected within the tract, and minimally affected tracts as those tracts with less than 20% of fixels affected within the tract.

2.7.3 | Region-of-Interest Volumetric Analysis

We performed volumetric analysis of subcortical and cerebellar ROIs to identify regions with significantly different volumes between subjects and controls. To do this, linear regression was performed on volumetric data from the 16 ROIs, with age and intracranial volume included as co-variants. Benjamini–Hochberg false discovery rate (FDR) correction was performed to determine statistical significance, adjusting for multiple comparisons across regions. Analysis of total brain volume and intracranial brain volume in individuals with PME compared to controls was also performed. All volumetric statistical analysis was performed in R (version 4.1.0).

3 | Results

3.1 | Demographics

Twelve individuals with PME were recruited. Only one individual (with spinal muscular atrophy-PME, UMRS = 291) was not able to tolerate the scan due to the severity of their myoclonus. We thus included 11 subjects, including two sibling pairs.

Subjects had a mean age at scan of 36 years (range 19–52). Controls ($n = 22$) were matched for age (mean 36 years, range 19–61, $p = 0.91$) and sex. Individual participant data regarding molecular genotype, clinical disease duration, and UMRS score at the time of scan are presented in Table 1. The majority ($n = 8$, 73%) had a diagnosis of ULD. The remaining participants had a variety of other types of PME. All subjects had a confirmed molecular diagnosis.

3.2 | Whole-Brain FBA

Analysis of structural connectivity revealed reduced FD, fiber bundle cross-section (FC), and the combined metric of FDC (FWE-corrected $p < 0.05$) throughout white matter tracts. Projection (thalamo-cortical, cortico-thalamic, and cortico-spinal tracts, thalamic radiations) and commissural fibers (splenium of corpus callosum) were areas of most severe involvement (Figure 1, panel A). Figure 1 shows the white matter tracts that exhibited a significant (FWE-corrected $p < 0.05$) reduction in FDC in the PME group when compared to controls. These fiber tracts are colored by effect size (percentage decrease in PME compared to controls) to demonstrate the white matter structures that exhibited prominent decreases in PME subjects.

Whole-brain FBA demonstrated involvement of the cerebellum and thalamus (Figure 1, panel B). Within the cerebellum, the superior cerebellar peduncles and the anterior cerebellar lobe (lobules I-V) were sites of particular involvement. The superior posterior cerebellar lobe and parts of the inferior posterior lobe

TABLE 1 | Clinical and molecular genotype data for subjects with PME.

Subject	PME syndrome	Genotype	Clinical disease duration (years)	Age at scan	UMRS score (/365)
1*	ULD	*CSTB* homozygous dodecamer repeat expansion	44	55	67
2	ULD	*CSTB* homozygous dodecamer repeat expansion	42	52	171
3*	ULD	*CSTB* homozygous dodecamer repeat expansion	38	48	76
4	ULD	*CSTB* homozygous dodecamer repeat expansion	31	46	39
5**	ULD	*CSTB* homozygous dodecamer repeat expansion	24	30	46
6**	ULD	*CSTB* homozygous dodecamer repeat expansion	20	23	72
7	ULD	*CSTB* homozygous dodecamer repeat expansion	13	24	165
8	ULD	*CSTB* compound heterozygote dodecamer repeat expansion and c.218_219delTC(p.Leu73fsX3)	40	51	163
9	AMRF	*SCARB2* homozygous c.1239 + 1G>T pathogenic variant	1	19	23
10	MEAK	*KCNC1* heterozygous c.959G>A (p.Arg320His) pathogenic variant	21	30	45
11	MERRF	*MT-TK* m.8344A>G	20	25	77

Note: *, **—sibling pairs.
Abbreviations: AMRF, action myoclonus renal failure syndrome; MEAK, myoclonus epilepsy and ataxia due to potassium channel mutation; MERRF, mitochondrial epilepsy with ragged red fibers; ULD, Unverricht-Lundborg Disease; UMRS, unified myoclonus rating scale.

(lobule VI, VIIa/b) were involved to a lesser extent. Within the thalamus, lateral thalamic structures (lateral thalamic nuclei) were more prominently involved than the anterior and medial thalamus. When only those individuals with ULD were included in the analysis, a similar pattern of white matter tract involvement was identified (see Figure S1).

3.3 | White Matter Tract Analysis

White matter tract analysis revealed that all 72 segmented white matter tracts were affected to some degree (magnitude of involvement 3%–56% of fixels within the tract exhibiting a significant decrease from whole-brain FBA). Figure 2 shows the white matter tracts that were severely affected (> 40% of fixels within the tract exhibiting a significant decrease in PME from whole-brain FBA) and those that were relatively preserved (< 20% of fixels within the tract exhibiting a significant decrease from whole-brain FBA). White matter tract analysis revealed that severely affected white matter tracts were predominantly posterior projection fibers in the cerebello-thalamo-cortical network, along with the left fornix and corpus callosum (Figure 2, panel A). In contrast, cortico-cortical association fiber pathways such as superior longitudinal fasciculus, arcuate, cingulate, and uncinate were relatively preserved (Figure 2, panel B).

3.4 | Region-Of-Interest Volumetric Analysis

After adjustment for multiple comparisons, seven ROIs demonstrated significantly reduced structural volumes in subjects with PME compared with controls (FDR $p < 0.05$). These were predominantly posterior structures, including the cerebellar cortex, white matter, and brainstem. The mid-anterior corpus callosum, hippocampus, thalamus, and ventral diencephalon also had significantly reduced structural volumes (Figure 3). There was no statistically significant difference in either total brain volume or intracranial brain volume between individuals with PME and healthy controls.

4 | Discussion

Application of advanced DWI analysis in this study reveals that individuals with PME have atrophy and changes in white matter fiber tracts, likely reflecting neuronal and axonal loss as part of a degenerative process. There is a distinctive pattern of white matter tract abnormality, with a dominant effect in cerebello-thalamo-cortical tracts, and smaller effects in other regions. Particular involvement of the motor system is noted both on FBA (corticospinal and cerebellar tracts) and volumetric analysis (mid-anterior corpus callosum, cerebellar cortex, and white matter and brainstem). These results accord well with earlier,

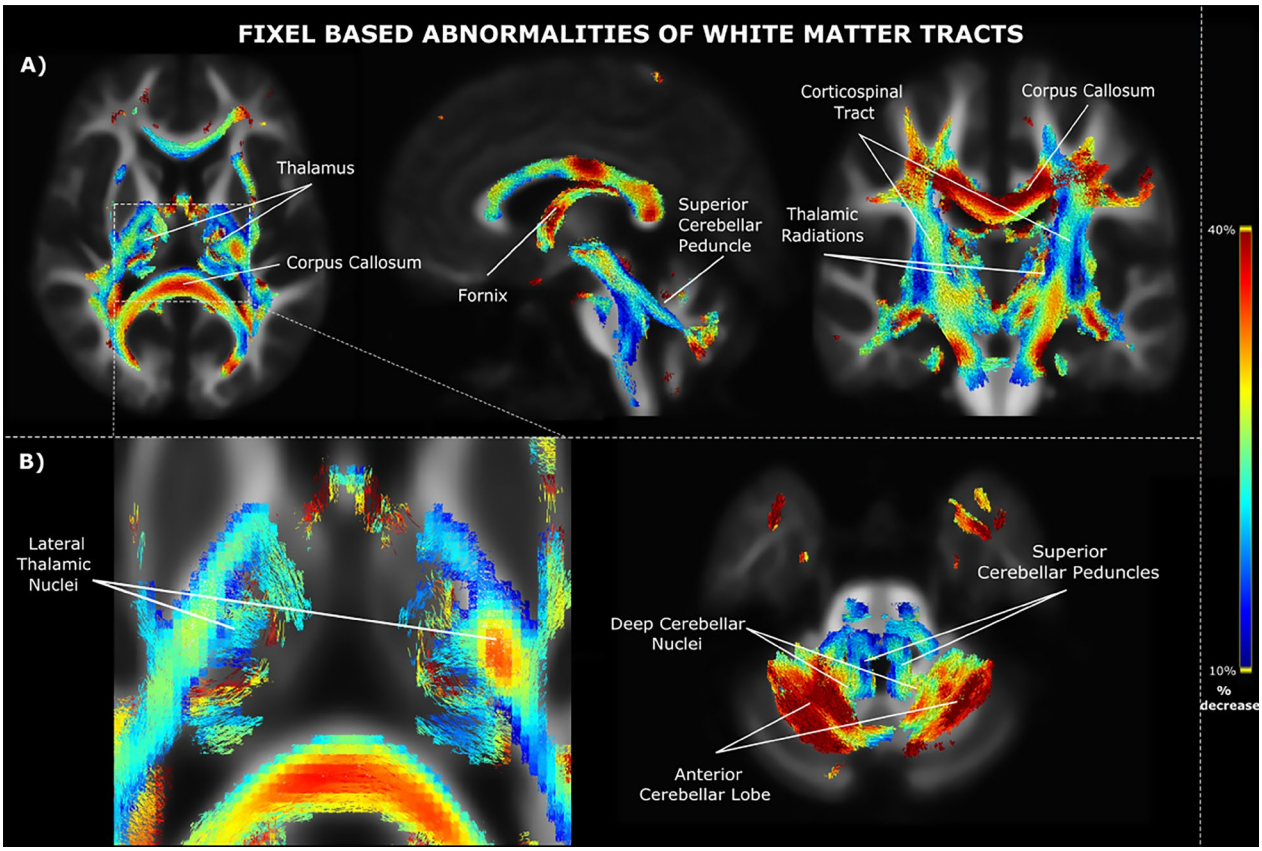

FIGURE 1 | Fixels exhibiting significant reductions in fiber density cross-section (FDC) in individuals with PME compared to controls (FWE corrected $p < 0.05$). Streamlines colored by percentage decrease compared to controls. Panel A—Axial, sagittal, and coronal images demonstrating the involvement of projection and commissural fibers. Panel B—Axial images demonstrating the pattern of thalamic involvement (noting particular involvement of lateral thalamic structures), and pattern of cerebellar involvement (noting particular involvement of anterior cerebellar lobe, superior cerebellar peduncles, and deep cerebellar nuclei).

more limited imaging analyses in PME which suggested significant brainstem and cerebellar involvement [11] and further expand our understanding of white matter involvement. Compared to milder, nonprogressive generalized epilepsy syndromes [29, 30], PME is associated with a more widespread pattern of white matter tract abnormality, with the most severe involvement of posterior projection fibers in the cerebello-thalamo-cortical network and relative preservation of association white matter tracts. This pattern of abnormality is consistent with the two predominant hypothesized mechanisms of PME, that is, either decreased inhibition of the cerebral cortex driven by cerebellar and brainstem dysfunction through thalamocortical loops [31–33] or decreased cerebral inhibitory activity involving corpus callosum and white matter tract projections [34]. Which may be the predominant mechanism is not able to be established at this stage. In future, the pattern of white matter abnormality may be able to be used as a biomarker or diagnostic tool and to guide the exploration of therapeutic interventions including neuromodulatory therapies.

The dominant white matter tract abnormality seen within the cerebello-thalamo-cortical network in PME accords well with the clinical and neurophysiological phenotypic features of this syndrome. The prominent clinical manifestation of ataxia is consistent with the involvement of the cerebellum, which, along with the thalamus, is affected in animal and human histopathological studies [4, 8]. Neurophysiological studies indicate that the myoclonus of PME is cortical in origin, attributed to decreased motor inhibition [35] or enhanced cortical neuron synchronization [36, 37]. Cortical thinning has been shown to correlate with the severity of myoclonus in ULD [38]. The cerebello-thalamo-cortical network is a well-recognized modulator of motor cortical excitability [39], and the severe white matter abnormality demonstrated within this network is a plausible key driver of the cortical hyper-excitability known to be underlying PME.

The only other study of white matter tracts in humans with PME revealed significantly decreased FA in almost all white matter tracts, suggesting that white matter is globally affected [14]. Correlation with animal imaging and histopathological data in that study suggested that the cerebellum and thalamus were sites of particular involvement. Results from our study are in concordance with this data but provide a more detailed delineation of the most severely affected white matter tracts in a fiber-specific manner, highlighting that not all brain regions are affected equally and that posterior projection tracts of the cerebello-thalamic network are most severely affected.

The most severely affected cerebellar structures are the superior cerebellar peduncles (SCP) as well as deep cerebellar nuclei. The SCP carry all efferent information from the cerebellum,

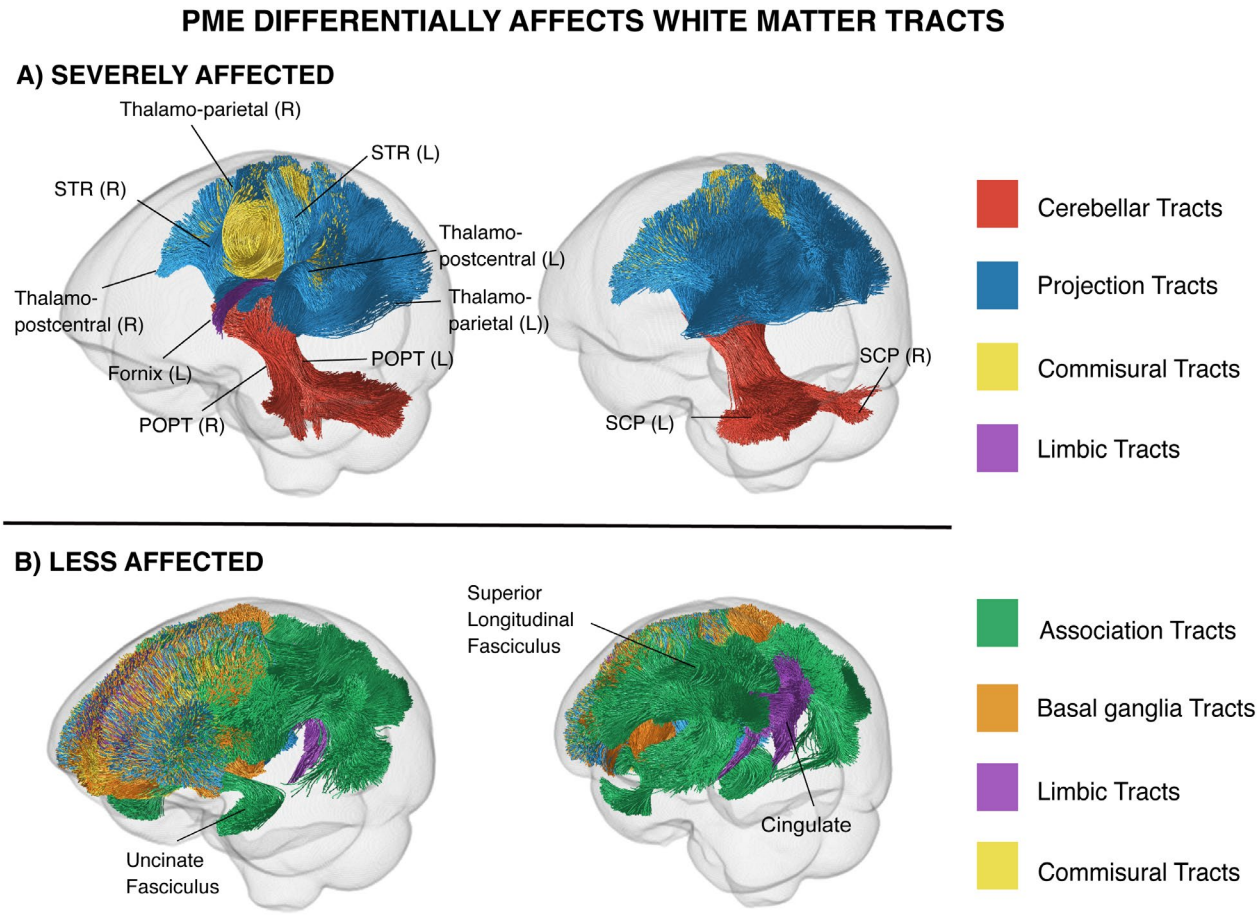

FIGURE 2 | White matter tract segmentation showing the percentage of significantly affected fixels per tract. Panel A—Glass brain images showing severely affected tracts (> 40% of fixels affected within the tract). Panel B—Glass brain images showing relatively preserved tracts (< 20% of fixels affected within the tract). POPT, parieto-occipital pontine tracts; SCP, superior cerebellar peduncle; STR, superior thalamic radiation.

comprised predominantly of excitatory glutamatergic projection neurons traveling from deep cerebellar nuclei and projecting to a variety of targets including descending motor tracts, cerebral cortex, and brainstem [40]. The deep cerebellar nuclei receive inhibitory input from Purkinje cells located in the cerebellar hemispheres. Our analysis highlights that the anterior cerebellar lobe seems to be preferentially involved within the cerebellum, and this lobe has important functional connectivity with the sensorimotor cortex [41]. Interestingly, a recent study of transcranial direct current cerebellar stimulation in individuals with cortical myoclonus facilitated sensorimotor cortex excitability, suggesting dysfunctional cerebello-thalamo-cortical input to the motor cortex [42]. Although cerebellar circuitry is complex, an imbalance of these processes caused by the demonstrated white matter tract abnormality in PME may result in cortical disinhibition and be an important factor driving the clinical phenotype.

Within the thalamus, lateral thalamic structures and superior thalamic radiations (connecting lateral thalamic nuclei to pre and postcentral gyri) are particularly involved, with relative sparing of medial structures. Lateral thalamic nuclei include ventral anterior (VA) and ventral posterior (VP) nuclei, both of which receive afferent fibers from basal ganglia structures and send efferent fibers to supplementary, premotor, and primary motor cortices [43]. The VP nucleus is the main relay nucleus for somatosensory pathways. White matter tract abnormality in these lateral thalamic structures could thus reasonably be expected to impact sensory processing and be relevant to stimulus-sensitive and action myoclonus.

We hypothesize that whilst in PME the white matter involvement is extensive, the large and dominant effect in the cerebello-thalamo-cortical networks is likely to be driving the clinical features that make up the PME phenotype. Analogies can be made with other progressive neurodegenerative conditions such as amyotrophic lateral sclerosis, where there is diffuse pathology but the distinguishing clinical phenotype arises due to targeted involvement of primary motor structures [44]. Work from our group has demonstrated similar, but less extensive, network abnormalities in other epilepsies, both generalized [45] and focal [46]. Interestingly, structural alterations in cerebello-thalamo-cortical tracts have recently been identified in familial adult myoclonic epilepsy (FAME), an epilepsy syndrome that shares some features with PME, namely myoclonus, GTCS, and giant SSEPs, though without the progressive neurological deterioration [47]. This supports the conceptualization that this network is key in driving some of the core clinical phenotypic features of PME.

All PMEs show progression with recurrent myoclonus and seizures. Disentangling whether the white matter tract abnormality is a primary pathology or a secondary consequence of recurrent seizure exposure is challenging. In neurodegenerative diseases, the combined metric FDC is most relevant, as it encompasses both

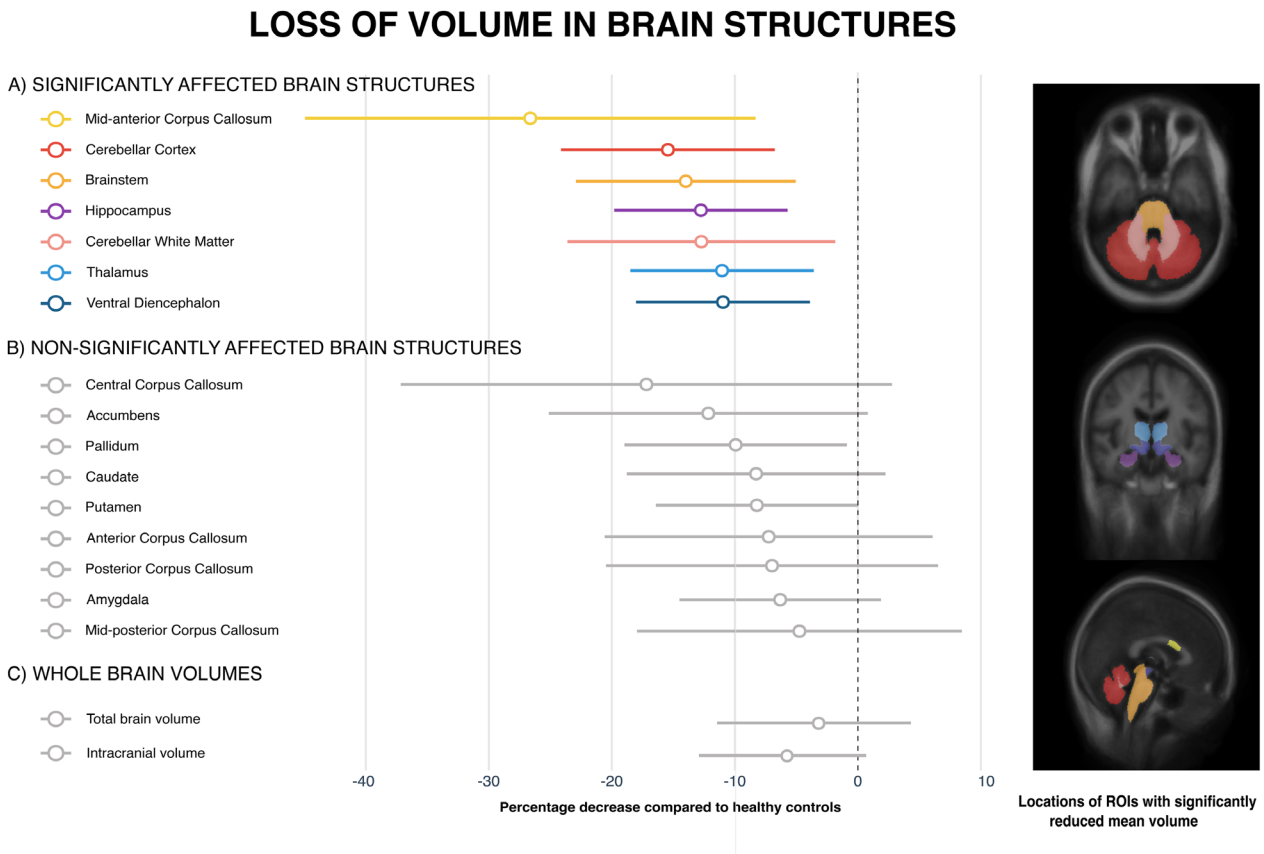

FIGURE 3 | ROI volumetric analysis of 16 ROIs, showing the percentage decrease compared to healthy control mean volume. Age and intracranial volume are included as covariates. ROIs with statistically significant differences in volume (FDR $p < 0.05$) compared to health controls after adjustment for multiple comparisons appear in color. Ventral diencephalon encompasses hypothalamus, subthalamic nuclei, mamillary body, substantia nigra, red nucleus, medial, and lateral geniculate nuclei.

atrophy due to accumulated axon loss (reflected in changes to fiber-bundle cross section) and the current state of the remaining white matter tissue (reflected in FD) [48]. Ultimately, longitudinal studies will be required to determine if the pattern of white matter tract abnormality alters with the progression of the disease.

The genetic basis of PME is well characterized, with now over 40 established genetic causes [49]. The pathological consequences of the genetic pathogenic variants are varied. How the heterogeneous genetic abnormalities associated with PME result in the white matter tract abnormalities, and why the cerebello-thalamo-cortical network has a specific vulnerability to more severe involvement will be important targets for basic science and animal-based studies going forward. The majority of our cohort has ULD, the most common form of PME. Although we were underpowered to explore each of the individual genetic etiologies within our PME cohort, the pattern of white matter involvement was very similar when the subgroup of individuals with ULD was analyzed. Further work will be able to examine whether there are particular patterns of white matter abnormality in individuals with different genetic causes of PME.

4.1 | Study Advantages and Limitations

Studies of PME present some special challenges. We have conducted this study with a well-defined cohort of an extremely rare epilepsy syndrome. A comprehensive, nationwide recruitment process over the 4-year study period was required to achieve this cohort, the final size of which reflects the rarity of the condition, especially in a country such as Australia. We do acknowledge, however, that the sample size of this study is small, and that a larger or replication sample would be ideal. This highlights the need for future collaborative pooling and analysis of MR data, as has been successfully performed in the study of other rare conditions and epilepsy syndromes [50, 51]. Furthermore, the clinical features associated with PME mean that successfully imaging this cohort can be extremely challenging, and particular attention was paid to minimizing the impact of motion both during the scan and in the analysis. Advanced MR analysis techniques developed at our center have been applied to the acquired data and allowed this challenging study to be performed.

5 | Conclusion

Individuals with PME have diffuse white matter tract abnormality, with a distinctive pattern of a dominant effect in the cerebello-thalamo-cortical tracts and smaller effects in other brain regions. This accords well with the characteristic clinical, neuropathological, and neurophysiological features of the PMEs. The mechanism by which the PME genes affect these tracts is not yet known. Ultimately, this pattern of white matter tract abnormality in PME informs our understanding of the

underlying pathophysiology of this devastating condition and may in future help guide potential new therapeutic targets, including exploration of neuromodulatory therapies.

Author Contributions

All authors (J.C, R.M, S.B., and G.J) were involved in the design and conceptualization of the study, data acquisition and analysis, and manuscript drafting, review, and completion.

Acknowledgments

Participants and families took part in the study. Florey Radiographers for expertise in facilitating MR imaging and acquisition. The Florey Institute of Neuroscience and Mental Health acknowledges support from the Victorian government and, in particular, funding from the Operational Infrastructure Support Grant. The authors acknowledge the facilities and technical assistance of the National Imaging Facility, a National Collaborative Research Infrastructure Strategy (NCRIS) capability, at the Florey Institute of Neuroscience and Mental Health. SFB is supported by an NHMRC Investigator Grant (APP1196637). GDJ is supported by the Australian Epilepsy Project, which received funding from the Australian Government under the Medical Research Future Fund (Frontier Health and Medical Research Program—Grant Numbers MRFF75908 and RFRHPSI000008) and the Victoria State Government (Victorian-led Frontier Health and Medical Research Program). Open access publishing facilitated by The University of Melbourne, as part of the Wiley - The University of Melbourne agreement via the Council of Australian University Librarians.

Conflicts of Interest

The authors declare no conflicts of interest.

Data Availability Statement

The data that support the findings of this study are available from the corresponding author upon reasonable request.

References

1. S. F. Berkovic, F. Andermann, S. Carpenter, and L. S. Wolfe, "Progressive Myoclonus Epilepsies: Specific Causes and Diagnosis," *New England Journal of Medicine* 315, no. 5 (1986): 296–305.

2. C. Courage, K. L. Oliver, E. J. Park, et al., "Progressive Myoclonus Epilepsies-Residual Unsolved Cases Have Marked Genetic Heterogeneity Including Dolichol-Dependent Protein Glycosylation Pathway Genes," *American Journal of Human Genetics* 108, no. 4 (2021): 722–738.

3. L. Canafoglia, S. Franceschetti, A. Gambardella, et al., "Progressive Myoclonus Epilepsies: Diagnostic Yield With Next-Generation Sequencing in Previously Unsolved Cases," *Neurology Genetics* 7, no. 6 (2021): e641.

4. M. Haltia, K. Kristensson, and P. Sourander, "Neuropathological Studies in Three Scandinavian Cases of Progressive Myoclonus Epilepsy," *Acta Neurologica Scandinavica* 45, no. 1 (1969): 63–77.

5. N. R. Cohen, S. R. Hammans, J. Macpherson, and J. A. Nicoll, "New Neuropathological Findings in Unverricht-Lundborg Disease: Neuronal Intranuclear and Cytoplasmic Inclusions," *Acta Neuropathologica* 121, no. 3 (2011): 421–427.

6. M. Koskiniemi, M. Donner, H. Majuri, M. Haltia, and R. Norio, "Progressive Myoclonus Epilepsy. A Clinical and Histopathological Study," *Acta Neurologica Scandinavica* 50, no. 3 (1974): 307–332.

7. P. Shannon, L. A. Pennacchio, M. K. Houseweart, B. A. Minassian, and R. M. Myers, "Neuropathological Changes in a Mouse Model of Progressive Myoclonus Epilepsy: Cystatin B Deficiency and Unverricht-Lundborg Disease," *Journal of Neuropathology and Experimental Neurology* 61, no. 12 (2002): 1085–1091.

8. L. A. Pennacchio, D. M. Bouley, K. M. Higgins, M. P. Scott, J. L. Noebels, and R. M. Myers, "Progressive Ataxia, Myoclonic Epilepsy and Cerebellar Apoptosis in Cystatin B-Deficient Mice," *Nature Genetics* 20, no. 3 (1998): 251–258.

9. P. Koskenkorva, J. Khyuppenen, E. Niskanen, et al., "Motor Cortex and Thalamic Atrophy in Unverricht-Lundborg Disease: Voxel-Based Morphometric Study," *Neurology* 73, no. 8 (2009): 606–611.

10. J. Hypponen, V. Paanila, M. Aikia, et al., "Progressive Myoclonic Epilepsy Type 1 (EPM1) Patients Present With Abnormal (1)H MRS Brain Metabolic Profiles Associated With Cognitive Function," *NeuroImage: Clinical* 39 (2023): 103459.

11. M. Mascalchi, R. Michelucci, M. Cosottini, et al., "Brainstem Involvement in Unverricht-Lundborg Disease (EPM1): An MRI and (1)H MRS Study," *Neurology* 58, no. 11 (2002): 1686–1689.

12. L. Canafoglia, C. Ciano, F. Panzica, et al., "Sensorimotor Cortex Excitability in Unverricht-Lundborg Disease and Lafora Body Disease," *Neurology* 63, no. 12 (2004): 2309–2315.

13. D. C. Reutens, A. Puce, and S. F. Berkovic, "Cortical Hyperexcitability in Progressive Myoclonus Epilepsy: A Study With Transcranial Magnetic Stimulation," *Neurology* 43, no. 1 (1993): 186–192.

14. O. Manninen, P. Koskenkorva, K. K. Lehtimaki, et al., "White Matter Degeneration With Unverricht-Lundborg Progressive Myoclonus Epilepsy: A Translational Diffusion-Tensor Imaging Study in Patients and Cystatin B-Deficient Mice," *Radiology* 269, no. 1 (2013): 232–239.

15. B. Jeurissen, J. D. Tournier, T. Dhollander, A. Connelly, and J. Sijbers, "Multi-Tissue Constrained Spherical Deconvolution for Improved Analysis of Multi-Shell Diffusion MRI Data," *NeuroImage* 103 (2014): 411–426.

16. G. Douaud, S. Jbabdi, T. E. Behrens, et al., "DTI Measures in Crossing-Fibre Areas: Increased Diffusion Anisotropy Reveals Early White Matter Alteration in MCI and Mild Alzheimer's Disease," *NeuroImage* 55, no. 3 (2011): 880–890.

17. S. J. Frucht, S. E. Leurgans, M. Hallett, and S. Fahn, "The Unified Myoclonus Rating Scale," *Advances in Neurology* 89 (2002): 361–376.

18. J. D. Tournier, R. Smith, D. Raffelt, et al., "MRtrix3: A Fast, Flexible and Open Software Framework for Medical Image Processing and Visualisation," *NeuroImage* 202 (2019): 116137.

19. J. Veraart, E. Fieremans, and D. S. Novikov, "Diffusion MRI Noise Mapping Using Random Matrix Theory," *Magnetic Resonance in Medicine* 76, no. 5 (2016): 1582–1593.

20. E. Kellner, B. Dhital, V. G. Kiselev, and M. Reisert, "Gibbs-Ringing Artifact Removal Based on Local Subvoxel-Shifts," *Magnetic Resonance in Medicine* 76, no. 5 (2016): 1574–1581.

21. N. J. Tustison, B. B. Avants, P. A. Cook, et al., "N4ITK: Improved N3 Bias Correction," *IEEE Transactions on Medical Imaging* 29, no. 6 (2010): 1310–1320.

22. J. L. R. Andersson and S. N. Sotiropoulos, "An Integrated Approach to Correction for Off-Resonance Effects and Subject Movement in Diffusion MR Imaging," *NeuroImage* 125 (2016): 1063–1078.

23. M. Bastiani, M. Cottaar, S. P. Fitzgibbon, et al., "Automated Quality Control for Within and Between Studies Diffusion MRI Data Using a Non-parametric Framework for Movement and Distortion Correction," *NeuroImage* 184 (2019): 801–812.

24. T. Dhollander, R. Mito, D. Raffelt, and A. Connelly, "Improved White Matter Response Function Estimation for 3-Tissue Constrained Spherical Deconvolution," *Proceedings of the International Society for Magnetic Resonance in Medicine* 27 (2019): 555.

25. D. Raffelt, J. D. Tournier, J. Fripp, S. Crozier, A. Connelly, and O. Salvado, "Symmetric Diffeomorphic Registration of Fibre Orientation Distributions," *NeuroImage* 56, no. 3 (2011): 1171–1180.

26. J. Wasserthal, P. Neher, and K. H. Maier-Hein, "TractSeg—Fast and Accurate White Matter Tract Segmentation," *NeuroImage* 183 (2018): 239–253.

27. B. Fischl, D. H. Salat, A. J. van der Kouwe, et al., "Sequence-Independent Segmentation of Magnetic Resonance Images," *NeuroImage* 23, no. 1 (2004): S69–S84.

28. M. Reuter, N. J. Schmansky, H. D. Rosas, and B. Fischl, "Within-Subject Template Estimation for Unbiased Longitudinal Image Analysis," *NeuroImage* 61, no. 4 (2012): 1402–1418.

29. J. O'Muircheartaigh, C. Vollmar, G. J. Barker, et al., "Abnormal Thalamocortical Structural and Functional Connectivity in Juvenile Myoclonic Epilepsy," *Brain* 135, no. 12 (2012): 3635–3644.

30. N. K. Focke, C. Diederich, G. Helms, M. A. Nitsche, H. Lerche, and W. Paulus, "Idiopathic-Generalized Epilepsy Shows Profound White Matter Diffusion-Tensor Imaging Alterations," *Human Brain Mapping* 35, no. 7 (2014): 3332–3342.

31. R. Eldridge, M. Iivanainen, R. Stern, T. Koerber, and B. J. Wilder, "Baltic Myoclonus Epilepsy: Hereditary Disorder of Childhood Made Worse by Phenytoin," *Lancet* 2, no. 8354 (1983): 838–842.

32. M. Habib, J. Roger, R. Khalil, et al., "Progressive Degenerative Myoclonic Epilepsy. Systematized Olivo-Cerebellar Lesions," *Revue Neurologique (Paris)* 141, no. 4 (1985): 274–288.

33. M. L. Koskiniemi, "Baltic myoclonus," *Advances in Neurology* 43 (1986): 57–64.

34. R. Michelucci, *Epilepsy and Movement Disorders*, ed. R. Guerrini (Cambridge University Press, 2002), 227–249.

35. L. Canafoglia, C. Ciano, E. Visani, et al., "Short and Long Interval Cortical Inhibition in Patients With Unverricht-Lundborg and Lafora Body Disease," *Epilepsy Research* 89, no. 2–3 (2010): 232–237.

36. E. Visani, P. Agazzi, L. Canafoglia, et al., "Movement-Related Desynchronization-Synchronization (ERD/ERS) in Patients With Unverricht-Lundborg Disease," *NeuroImage* 33, no. 1 (2006): 161–168.

37. F. Panzica, L. Canafoglia, and S. Franceschetti, "EEG-EMG Information Flow in Movement-Activated Myoclonus in Patients With Unverricht-Lundborg Disease," *Clinical Neurophysiology* 125, no. 9 (2014): 1803–1808.

38. P. Koskenkorva, E. Niskanen, J. Hypponen, et al., "Sensorimotor, Visual, and Auditory Cortical Atrophy in Unverricht-Lundborg Disease Mapped With Cortical Thickness Analysis," *AJNR. American Journal of Neuroradiology* 33, no. 5 (2012): 878–883.

39. Y. Ugawa, B. L. Day, J. C. Rothwell, P. D. Thompson, P. A. Merton, and C. D. Marsden, "Modulation of Motor Cortical Excitability by Electrical Stimulation Over the Cerebellum in Man," *Journal of Physiology* 441 (1991): 57–72.

40. M. L. Streng and E. Krook-Magnuson, "The Cerebellum and Epilepsy," *Epilepsy & Behavior* 121 (2021): 106909.

41. R. L. Buckner, F. M. Krienen, A. Castellanos, J. C. Diaz, and B. T. Yeo, "The Organization of the Human Cerebellum Estimated by Intrinsic Functional Connectivity," *Journal of Neurophysiology* 106, no. 5 (2011): 2322–2345.

42. A. Latorre, L. Rocchi, G. Paparella, N. Manzo, K. P. Bhatia, and J. C. Rothwell, "Changes in Cerebellar Output Abnormally Modulate Cortical Myoclonus Sensorimotor Hyperexcitability," *Brain* 147, no. 4 (2024): 1412–1422.

43. J. O'Muircheartaigh, S. S. Keller, G. J. Barker, and M. P. Richardson, "White Matter Connectivity of the Thalamus Delineates the Functional Architecture of Competing Thalamocortical Systems," *Cerebral Cortex* 25, no. 11 (2015): 4477–4489.

44. D. W. Cleveland and J. D. Rothstein, "From Charcot to Lou Gehrig: Deciphering Selective Motor Neuron Death in ALS," *Nature Reviews. Neuroscience* 2, no. 11 (2001): 806–819.

45. G. S. F. Jackson, P. Carney, D. Raffelt, F. Calamante, and A. Connelly, "Structural Connectivity Changes in Refractory Childhood Absence Epilepsy," *International Society for Magnetic Resonance in Medicine*; Singapore (2016): 771.

46. R. Mito, D. N. Vaughan, M. Semmelroch, A. Connelly, and G. D. Jackson, "Bilateral Structural Network Abnormalities in Epilepsy Associated With Bottom-Of-Sulcus Dysplasia," *Neurology* 98, no. 2 (2022): e152–e163.

47. B. Wang, H. Wang, Z. Cen, et al., "White Matter Alterations in Familial Cortical Myoclonic Tremor With Epilepsy Type 1," *Epilepsia* 63, no. 5 (2022): 1093–1103.

48. D. A. Raffelt, J. D. Tournier, R. E. Smith, et al., "Investigating White Matter Fibre Density and Morphology Using Fixel-Based Analysis," *NeuroImage* 144 (2017): 58–73.

49. K. L. Oliver, I. E. Scheffer, M. F. Bennett, B. E. Grinton, M. Bahlo, and S. F. Berkovic, "Genes4Epilepsy: An Epilepsy Gene Resource," *Epilepsia* 64 (2023): 1368–1375.

50. T. J. R. Rezende, I. M. Adanyeguh, F. Arrigoni, et al., "Progressive Spinal Cord Degeneration in Friedreich's Ataxia: Results From ENIGMA-Ataxia," *Movement Disorders* 38, no. 1 (2023): 45–56.

51. S. N. Hatton, K. H. Huynh, L. Bonilha, et al., "White Matter Abnormalities Across Different Epilepsy Syndromes in Adults: An ENIGMA-Epilepsy Study," *Brain* 143, no. 8 (2020): 2454–2473.

Supporting Information

Additional supporting information can be found online in the Supporting Information section.